Thermoelectric properties of electron doped $SrO(SrTiO_3)_n$ (n=1,2) ceramics

Yifeng Wang,[1] Kyu Hyoung Lee,[2,a)] Hiromichi Ohta,[1,2] and Kunihito Koumoto[1,2,b)]
[1]*Graduate School of Engineering, Nagoya University, Furo-cho, Chikusa, Nagoya 464-8603, Japan*
[2]*CREST, Japan Science and Technology Agency, 4-1-8 Honcho, Kawaguchi 332-0012, Japan*

(Received 26 October 2008; accepted 18 March 2009; published online 18 May 2009)

Crystal structure and thermoelectric properties of Nb^{5+}- and Ln^{3+}-(rare earth: La^{3+}, Nd^{3+}, Sm^{3+}, and Gd^{3+}) doped $SrO(SrTiO_3)_n$ (n=1,2) ceramics, which were fabricated by conventional hot-pressing, were measured to clarify the effects of Ti^{4+}- and Sr^{2+}-site substitution on the thermoelectric properties. The thermal conductivities are very close between the n=1 and 2 phases either doped with Nb^{5+} or Ln^{3+} and decreased by ~60% at room temperature and ~30% at 1000 K as compared to that of $SrTiO_3$, which is likely due to an enhanced phonon scattering at the $SrO/(SrTiO_3)_n$ (n=1,2) interfaces. The density of states effective mass m_d^* (1.8–2.4 m_0) and consequently the Seebeck coefficient $|S|$ in Nb^{5+}-doped samples are fairly smaller than those reported for $SrTiO_3$, which probably resulted from a deterioration of DOS due to the formation of the singly degenerate a_{1g} (Ti $3d_{xy}$) orbital as the conduction band bottom, which should be induced by the distortion of TiO_6 octahedra in $(SrTiO_3)_n$ layers. However, in the Ln^{3+}-doped $SrO(SrTiO_3)_2$, the TiO_6 octahedra were found to be restored, in contrast to the Nb^{5+}-doped, with a gradually increasing O–Ti–O bond angle in the (100) plane at high temperatures, which would lead to the formation of triply degenerate Ti $3d$-t_{2g} (d_{xy}, d_{yz}, and d_{xz}) orbitals to cause a significant enhancement in m_d^* (~7.5 m_0 at 1000 K) and consequently in $|S|$. Accordingly, the maximum dimensionless figure of merit ZT~0.24 obtained in 5%-Gd^{3+}-doped $SrO(SrTiO_3)_2$ at 1000 K is about 70% larger than that of Nb-doped $SrO(SrTiO_3)_2$ ($ZT_{1000\ K}$~0.14). © *2009 American Institute of Physics*. [DOI: 10.1063/1.3117943]

I. INTRODUCTION

Thermoelectric (TE) performance is essentially evaluated with the dimensionless TE figure of merit $ZT=S^2\sigma T\kappa^{-1}$, where Z, S, σ, and κ are the figure of merit, Seebeck coefficient, electrical conductivity, and thermal conductivity at a given absolute temperature (T), respectively, and $ZT \geq 1$ is regarded as a criteria of practical application. Recently, Ti-based oxides such as La^{3+}- or Nb^{5+}-doped $SrTiO_3$ (STO),[1–3] and Nb^{5+}-doped TiO_2 have received increasing attention for the realization of TE energy conversion devices operating at high temperatures because they are basically stable at such temperatures.

Although 20% Nb^{5+}-doped $SrTiO_3$ exhibits the highest power factor $S^2\sigma$ at 1000 K (~1.3 mW m^{-1} K^{-2}) among Ti-based oxides, the ZT value is not sufficiently enough ($ZT_{1000\ K}$=0.37) for practical TE power generation because the κ-value (~12 W m^{-1} K^{-1} at 300 K and 3 W m^{-1} K^{-1} at 1000 K) is quite high due most likely to the high phonon frequencies of O^{2-} ions that are the major constituent in oxides. In order to overcome this issue, we chose a layered perovskite-type Ruddlesden-Popper (RP) phase, $SrO(SrTiO_3)_n$ (n=integer) as a promising candidate to realize a high ZT because, generally, layered oxides, e.g., some cobaltites and $In_2O_3(ZnO)_m$,[6–8] often exhibit small κ-value.

Figures 1(a) and 1(b) show the schematic crystal structures of $SrO(SrTiO_3)_n$ (n=1,2),[9,10] which are regarded as a superlattice of SrO layers and $(SrTiO_3)_n$ slabs alternately stacking along the c-axis. We expected that $SrO(SrTiO_3)_n$ exhibits lower κ value than that of $SrTiO_3$ because the interfaces between SrO layers and $(SrTiO_3)_n$ slabs may enhance the phonon scattering. In the previous report,[5] we clarified that the κ-values of Nb-doped $SrO(SrTiO_3)_n$ (n=1,2) were significantly small as compared to that of $SrTiO_3$ crystal ($\kappa_{SrO(SrTiO_3)n}/\kappa_{SrTiO_3}$ ~0.5 at 300 K).

However, the $|S|$ values of Nb^{5+}-doped $SrO(SrTiO_3)_2$ were rather small as compared to those of $SrTiO_3$ due to the fact that the density of states (DOS) of $SrO(SrTiO_3)_2$ is smaller than those of $SrTiO_3$. Although the bottom of the conduction band (CB) for $SrTiO_3$ is composed of triply degenerate Ti $3d$-t_{2g} orbitals,[11] that of $SrO(SrTiO_3)_2$ is composed of nondegenerate a_{1g} orbital since the TiO_6 octahedra of $SrO(SrTiO_3)_n$ [Figs. 1(c) and 1(d)] crystal are deformed either by positioning the surrounding O atoms with different distances from the Ti atom or by shifting the Ti atoms slightly to SrO layer side, though that of $SrTiO_3$ is symmetrical with the Ti atom at the center and the O(3)–Ti–O(3) bond angle of 180°. This distortion induces the crystal field splitting of Ti $3d$-t_{2g} orbitals (d_{xy}, d_{yz}, and d_{xz}) into e_g (d_{yz} and d_{xz})-a_{1g} (d_{xy}) orbitals.[12] Thus, lattice engineering such as site substitution is essentially important to restore the bond angle of $SrO(SrTiO_3)_2$ crystal to 180°.

In the previous letter,[13] we briefly reported that 5% Sm^{3+}-substituted $SrO(SrTiO_3)_2$ ceramics exhibit larger $|S|$ values due to the fact that the bond angle of O(3)–Ti–O(3)

a)Present address: Materials Research Laboratory, Samsung Advanced Institute of Technology, P.O. Box 111, Suwon, Korea.
b)Author to whom correspondence should be addressed. Electronic mail: koumoto@apchem.nagoya-u.ac.jp.

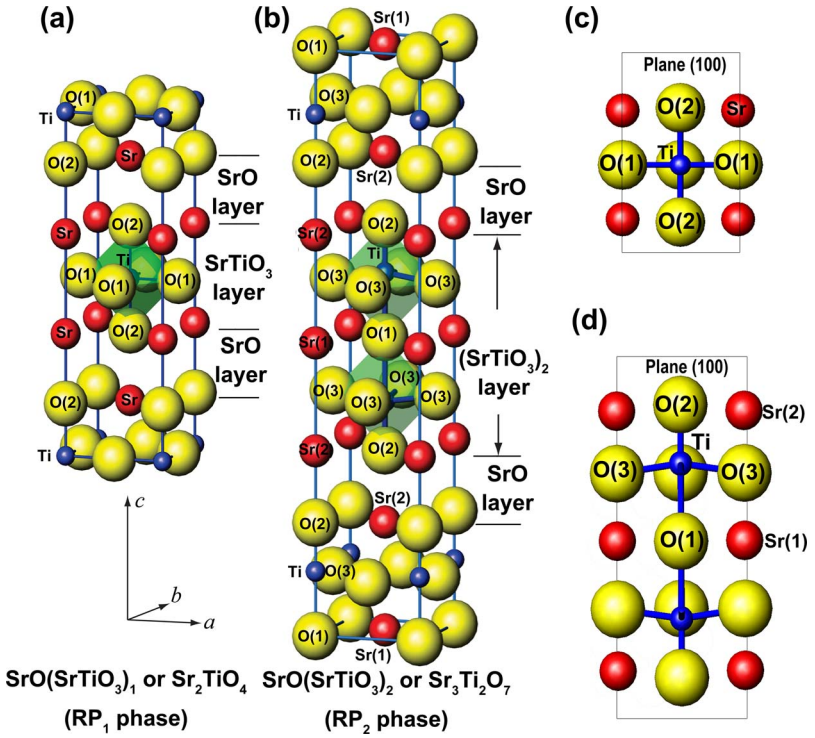

FIG. 1. (Color online) Schematic crystal structures of Ruddlesden–Popper phase, $SrO(SrTiO_3)_n$ with (a) $n=1$ and (b) $n=2$, and of TiO_6 octahedra in (c) $n=1$ compound with an O(1)–Ti–O(1) bond angle of 180° and two different Ti–O bonds and (d) $n=2$ compound with a O(3)–Ti–O(3) bond angle of ~177° and three different Ti–O bonds.

for 5% Sm^{3+}-substituted $SrO(SrTiO_3)_2$ is 179° at 300 K and 180° at 800 K, while that of $SrO(SrTiO_3)_2$ was always 177°. This paper provides a detailed description of TE properties of two series of RP compounds: Nb^{5+} (Ti-site)-doped[5] and/or Ln^{3+} (rare earth: Gd^{3+}, Sm^{3+}, Nd^{3+}, and La^{3+}; Sr^{2+}-site)-doped $SrO(SrTiO_3)_n$ ($n=1,2$) (Ref. 14) and their relationship to the crystal structures.

II. SAMPLE PREPARATION

The two series of n-type $SrO(SrTiO_3)_n$ (hereafter RP_n; $n=1,2$) that are doped with Nb^{5+}- for Ti^{4+}-sites [$SrO(SrTi_{1-x}Nb_xO_3)_n$, $x=0.05-0.2$, $n=1,2$; hereafter $100x$-Nb-RP_n] and with rare earth metals for Sr^{2+}-sites [$(Sr_{1-x}Ln_x)_{n+1}Ti_nO_{3n+1}$, $x=0.05$, 0.1; $n=1,2$; $Ln^{3+}=Gd^{3+}$, Sm^{3+}, Nd^{3+}, and La^{3+}; hereafter $100x$-Ln-RP_n) were fabricated by a conventional solid-state reaction that was followed by a hot-pressing process. First, fine starting chemical powders of $SrCO_3$, TiO_2, Nb_2O_5, and Ln_2O_3 (Ln=Gd, Sm, Nd, and La) (Kojundo Chemical Laboratory Co.) in a stoichiometric proportion were thoroughly mixed by using a planetary mill for ~1 h with some pure ethanol solution and a mount of yttria-stabilized ZrO_2 beads inside a Teflon® pot. After being dried at ~100 °C, the mixture was preheated at ~1200 °C for 12 h twice with an intermediate grinding to decarbonate and homogenize the reactants and to initialize the formation of RP phases. Then the mixture was sintered in a graphite crucible in a flow of Ar gas (~20 ml min^{-1}) at ~1450 °C for ~2 h several times until a single phase state was confirmed by powder x-ray diffraction (XRD) measurement. In fact, the RP_2 phase is the stablest one among the STO RP_n (n=integer) phase[15] and was indeed experimentally synthesized with single phase either Nb- or Ln (doping level $x \leq 0.05$)-doped, while the RP_1 phase contained a tiny amount of RP_2 impurity. Finally, a mount of power sample (~40 g) was hot-pressed in an Ar atmosphere at ~1450 °C for ~1 h under 36 MPa into highly dense ceramic samples (around 96%–99% of the theoretical density). As confirmed by scanning electron microscopy and XRD observations, the samples are basically free from preferential crystallographic orientations and texturation.

III. RESULTS AND DISCUSSION

A. TE properties

The S and σ values were measured simultaneously by a conventional steady state method and a four-probe method, respectively, in an Ar atmosphere at 300–1000 K. The carrier concentration n_e was determined by Hall effect measurement with a van der Pauw electrode configuration under vacuum (~10^{-3} Pa) over a same temperature range. The heat capacity C_p and the thermal diffusivity α were measured by differential scanning calorimetry in air and laser-flash method under vacuum, respectively, to estimate the κ ($\kappa=\alpha\rho C_p$, where ρ is the bulk density). The main TE properties for $100x$-Nb-RP_n ($x=0.05-0.2$, $n=1,2$) and $100x$-Ln-RP_n ($x=0.05$; Ln=Gd,Sm,Nd; and La; $n=1,2$) are summarized in Figs. 2–4, respectively.

B. Thermal conductivity κ

Shown in Figs. 2(a) and 3(a) are the comparison of κ-values between $SrTiO_3$ (the $n=\infty$ RP compound) and doped-RP_n ($n=1,2$). Clearly seen is the remarkable reduc-

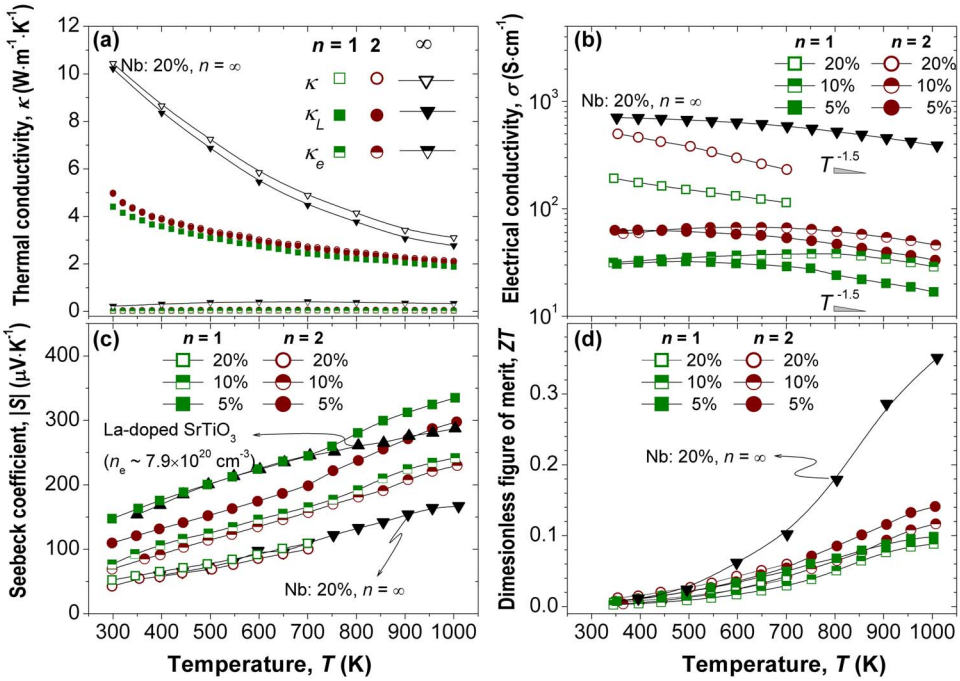

FIG. 2. (Color online) Temperature dependence of (a) the thermal conductivity κ, (b) electrical conductivity σ, (c) Seebeck coefficient S, and (d) the dimensionless figure of merit ZT in Nb-doped $SrO(SrTi_{1-x}Nb_xO_3)_n$ (x=0.05–0.2, n=1,2).

tion in κ of the RP_n phases as compared to that of $SrTiO_3$ by ~60% at room temperature and ~30% at 1000 K. In light of the small contribution of electrons κ_e (~0.3 W m^{-1} K^{-1}) in the RP_n-phases, which were calculated following the Wiedemann–Franz law from the determined S and σ data as described elsewhere,[5] it is reasonable to deduce that this reduction in κ is mainly due to the enhanced phonon scattering probably caused by the numerous $SrO/(SrTiO_3)_n$ interfaces. Therefore, Nb- and Ln-doped RP_n (n=1,2) compounds differ little in thermal transport properties, which should be due to their similar crystal structures that dominates κ_L, the primary portion of κ.

C. Electrical conductivity σ

Electrical conductivities of Nb-RP_n are shown in Fig. 2(b). It can be seen that the σ-values in Nb-RP_n-phases in-

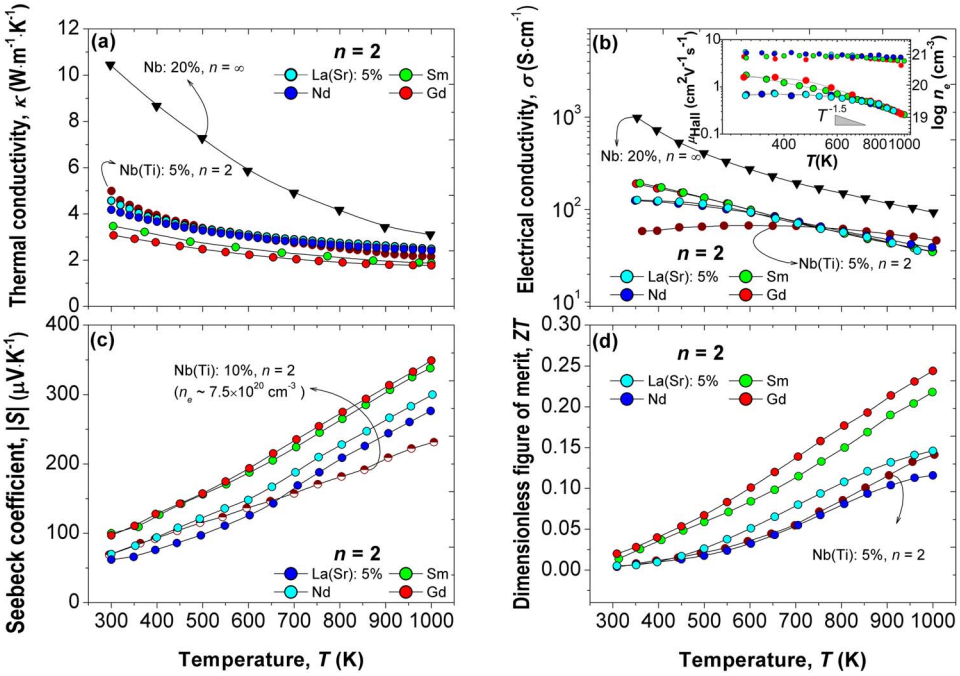

FIG. 3. (Color online) Temperature dependence of (a) the thermal conductivity κ, (b) electrical conductivity σ, (c) Seebeck coefficient S, and (d) the dimensionless figure of merit ZT in 5%-Ln^{3+}-doped $SrO(SrTiO_3)_2$ (Ln^{3+}=Gd^{3+}, Sm^{3+}, Nd^{3+}, and La^{3+}). The inset in (b) shows the Hall mobility in the whole temperature range.

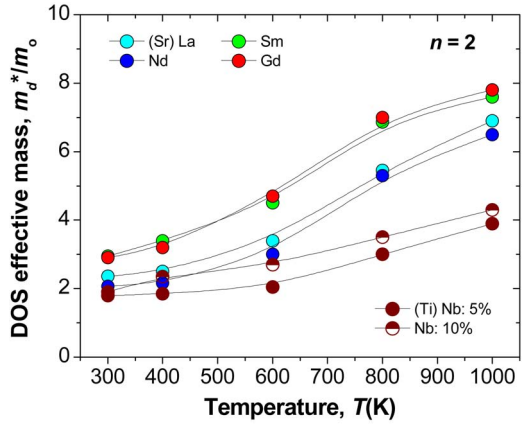

FIG. 4. (Color online) DOS effective mass m_d^* in the 5%-Ln^{3+} (Ln^{3+} = Gd^{3+}, Sm^{3+}, Nd^{3+}, and La^{3+})-, 5% and 10%-Nb-doped $SrO(SrTiO_3)_2$ as a function of temperature.

crease generally with Nb doping level reflecting the role of Nb as an electron donor. Furthermore, the σ-value in STO and Nb-RP_n ($n=1,2$) containing similar n_e shows an order of magnitude as $\sigma_{\text{Nb-STO}} > \sigma_{\text{Nb-RP}_2} > \sigma_{\text{Nb-RP}_1}$, reflecting the role of SrO layers as insulating barriers, which concludes that the electron conduction in the RP phases takes place predominantly along the $SrTiO_3$ layers. The similarities have been reported as well in some other RP systems.[16,17] Above 750 K, the σ-values drop proportionally to $T^{-1.5}$ in 100x-Nb-RP_n phases ($x=0.05-0.2$, $n=1,2$) such as in $SrTi_{0.8}Nb_{0.2}O_3$,[2,3] which additionally support the above conclusion on the role of $SrTiO_3$ layers as the main conduction passage. Apparently, one can see from Fig. 3(b) that the σ values in 5-Ln-RP_2 are quite close to that of 10-Nb-RP_2 containing a close n_e, also with a same temperature dependence above 750 K [inset of Fig. 3(b)], which is to say that the electron conductions in the both RP series are very similar. Thereby, we presume Ln^{3+}- and Nb^{5+}-doping in the RP phases differ little in their effects on σ as well as observed in thermal conductivities.

D. Seebeck coefficient |S|

The S-T curves of 100x-Nb-RP_n ($x=0.05-0.2$, $n=1,2$) and 5-Ln-RP_n samples are presented in Figs. 2(c) and 3(c), respectively. The S values are all negative, suggesting the n-type conduction in all samples. As a whole, the $|S|$ values are smaller in higher n_e-containing compounds and decrease with temperature. It should be noted that as shown in Fig. 3(c), even at a smaller n_e, Nb-RP phase's $|S|$ values are lower than those of $SrTiO_3$ [e.g., La-doped[1] $SrTiO_3$ with $n_e \sim 7.9 \times 10^{20}$ cm^{-3} has $|S|$ rather larger than that of 10-Nb-RP_n ($n=1,2$) (Ref. 5) with $n_e \sim 7.5 \times 10^{20}$ cm^{-3} over the whole temperature range], with $|S|$ in RP_1 relatively higher than those in Nb-RP_2. Furthermore, by a comparison between the data for Ln-RP_2 and 10-Nb-RP_2 shown in Fig. 3(c), it can be clearly seen that the $|S|$ values are rather larger than those of Nb-RP_2; furthermore they increase at a much larger rate against temperature for the former than those for the latter even though at a close n_e, especially in Gd- and Sm-RP_2 at high temperatures. These particularities are further discussed in the following context.

E. Dimensionless figure of merit ZT

Figures 2(d) and 3(d) represent the dimensionless figure of merit ZT of Nb-RP_n and Ln-RP_n as a function of temperature, respectively. Overall, the values increase progressively with temperature and arrive to the maximums ranging 0.1–0.24 at 1000 K. For Nb-RP_n, the ZT values are a little higher in RP_2 than in RP_1 with a close n_e, as mainly favored by their larger σ as to compensate their inferiority in $|S|$. However, even the maximum $ZT_{1000\ \text{K}} \sim 0.14$ obtained in 5-Nb-RP_2 is no more than 30% of $ZT_{1000\ \text{K}} \sim 0.37$ reported for 20-Nb-STO,[5] which suggests that the decrease in $S^2\sigma$ overwhelms the contribution of the reduction in κ. Inspiringly, for Ln-RP_2, thanks to the significant increase in $|S|$, the ZTs are remarkably enhanced to reach a maximum of $ZT_{1000\ \text{K}} \sim 0.24$ in 5-Gd-RP_2, which is about 70% larger than that of Nb-RP_2 and is even slightly higher than 5-Nb-STO ($ZT_{1000\ \text{K}} \sim 0.22$).[5]

F. Crystal structures

In order to clarify the origin of $|S|$ enhancement by the Ln substitution, we investigated the crystal structures because the shape of TiO_6 octahedron strongly affects electronic structure of the bottom of the CB as described above. Structural parameters of the crystal structures for the final products were derived from the Rietveld refinement using the RIETAN-2000 program[18] on the powder XRD patterns finely collected at room temperature (RINT 2000, Rigaku Co.) and in a 300–1000 K temperature range (SmartLab, Rigaku Co).

Figure 5 shows the structural parameters for Nb-RP_n and Ln-RP_n crystal lattices and TiO_6 octahedra as functions of the dopant's specific ionic radius (here referred to as the ionic radius ratio of Ln^{3+} to that of Sr^{2+} or that of Nb^{5+} to Ti^{4+} basing on the data from Ref. 19). Generally, the crystal lattice parameters a, c, and the lattice volume V increase in the both RP compounds with the specific ionic radius and/or Nb-doping level [Figs. 5(a) and 5(b)], which is self-evident when substituted with bigger dopant cation either of Nb^{5+} or Ln^{3+}.

More important are the structural features relating to the TiO_6 octahedra symmetry in the RP phases. In RP_1 compounds, the O(1)–Ti–O(1) bond angle in the (100) plane is always equal (180°) for Nb- and Ln-doped series. Besides, the Ti–O(1,2) bond lengths tend to converge with increasing specific dopant cation radius, which means a higher symmetry of the TiO_6 in Nb-RP_1 than Ln-RP_1 (crystal structural data for Nb-RP_n are recited from Refs. 5 and 20).

On the other hand, for the RP_2 phases, the Ti–O(1–3) bond lengths tend to converge when doped with Ln^{3+} of small radius, while they diverge when doped with increasing level of Nb. Moreover, although the O(3)–Ti–O(3) band angle in the (100) plane almost remains constant for the undoped compound[20] and that in Nb-RP_2 decreases as temperature arises to further deteriorate the local symmetry state of the TiO_6 octahedra, the O(3)–Ti–O(3) angle in Sm-RP_2 contrastingly grows gradually with increasing temperature from ~179° at room temperature to ~180° at 800 K (Fig. 6), which is presumed to be a result of the preferential occupa-

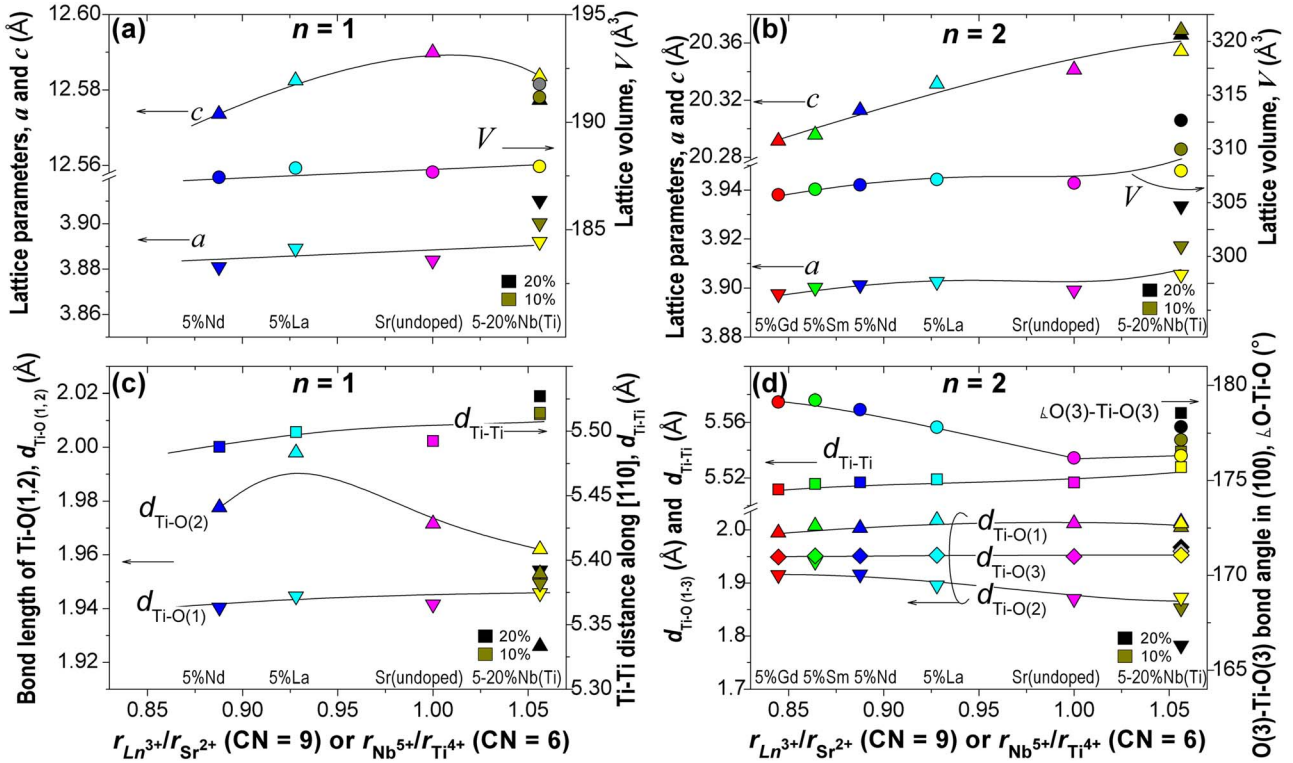

FIG. 5. (Color online) The lattice parameters of crystal structures [(a) and (b)] and the structural parameters for TiO_6 [(c) and (d)] in Nb^{5+}- and Ln^{3+}-doped $SrO(SrTiO_3)_n$ ($n=1,2$) as functions of the specific radii (hereby the radius ratio of Nb^{5+} to Ti^{4+} and of Ln^{3+} to Sr^{2+}).

tion of Ln^{3+} at the 12-coordinate Sr-site in the perovskite layers that was confirmed by the Rietveld refinement and is similar to the findings for some other RP-type compounds.[21–23] These two structural modifications would cause the inherently distorted TiO_6 octahedra to restore, which is clearly to say small-sized-Ln-doping in RP_2 would recover the irregular TiO_6 octahedra, especially at high temperatures, to a high symmetry state, which is a characteristic of those in $SrTiO_3$.

G. Relationship between |*S*| and O(3)–Ti–O(3) band angle

Accordingly, the degeneration state of Ti $3d$-t_{2g} orbitals should be different in Nb-RP_2 and Ln-RP_2. For Nb-RP_2, as a result of low TiO_6 symmetry, the Ti $3d$-t_{2g} orbitals would further split to a singly degenerate a_{1g} level consisting of $3d_{xy}$ at a lower energy state forming the lower CB bottom and a doubly degenerate level consisting of $3d_{yz}$ and $3d_{xz}$ orbitals with higher energy, which usually happens to irregularly coordinate octahedra.[4,24] For Ln-RP_2, however, where the TiO_6 octahedra are restored to a highly symmetrical shape, the $3d_{yz}$ and $3d_{xz}$ orbitals would also be shift to join the $3d_{xy}$ orbital at the CB bottom to form a triply degeneracy state of Ti $3d$ orbitals as in STO.[11]

From these results, we speculate that the behavior of m_d^* for the RP phases as (1) the relatively larger m_d^* in RP_1 than in RP_2 is a result of the higher symmetry of TiO_6 octahedra in RP_1 despite of their shorter Ti–Ti distance than those of RP_2 and (2) the m_d^* in Ln-RP_2 heavier than those in Nb-RP_2 reveals the significant effect of the local symmetry of TiO_6 on the enhancement in m_d^* and S rather than the Ti–Ti distance in RP_2 phases. Nevertheless, one still can find the limited increase in m_d^* for Nb-RP_2, which should be attributed to a secondary effect of the thermal expansion of Ti–Ti distance according to the previous findings. Therefore, we conclude that the m_d^* value is primarily related to local symmetry of TiO_6, especially the O(3)–Ti–O(3) bond angle in the (100) plane in RP phases, and secondarily to the Ti–Ti distance along the [110] direction, as schematically illustrated in Fig. 7.

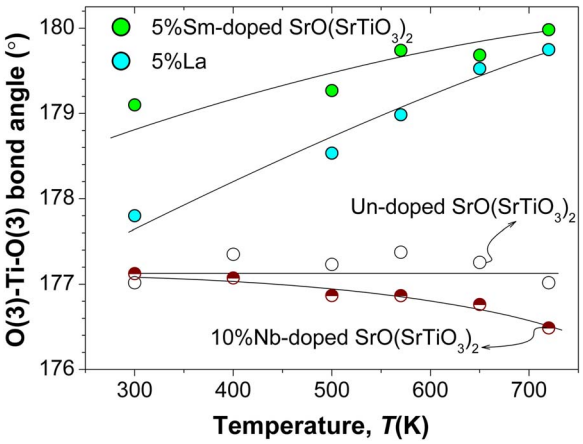

FIG. 6. (Color online) Temperature dependence of O(3)–Ti–O(3) bond angle in the (100) plane for undoped, 5%-Ln^{3+} (Sm^{3+} and La^{3+})-, and 10%-Nb^{5+}-doped $SrO(SrTiO_3)_2$.

IV. SUMMARY

Crystal structure and TE properties of Nb^{5+}- and Ln^{3+} (rare earth: La^{3+}, Nd^{3+}, Sm^{3+}, and Gd^{3+})-doped $SrO(SrTiO_3)_n$ ($n=1,2$) ceramics, which were fabricated by

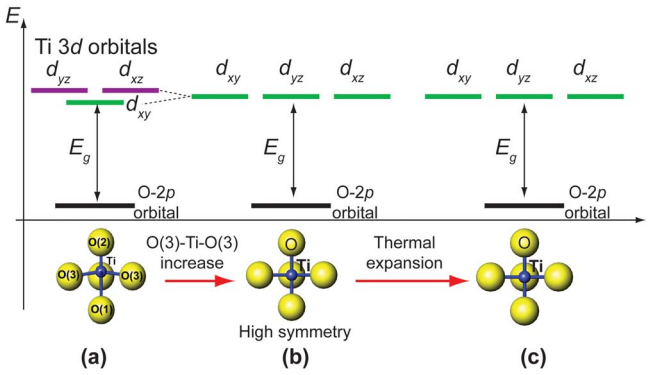

FIG. 7. (Color online) Schematic illustration of the structural restoration in TiO_6 in $SrO(SrTiO_3)_n$ ($n=2$) and its accompanying effect on the degeneracy state of Ti $3d$-t_{2g} orbital. Thanks to Ln^{3+}-doping at Sr^{2+}-site, the TiO_6 octahedra at low temperature (a) would be restored to a high symmetry state (b) and experience a thermal expansion (c) that leads to the lengthened Ti–Ti distance in [110] direction.

conventional hot-pressing, were measured to clarify the effects of Ti^{4+}- and Sr^{2+}-site substitution on the TE properties. The thermal conductivities are very close between the $n=1$ and 2 phases doped with either Nb^{5+} or Ln^{3+}, decreased by ~60% at room temperature and ~30% at 1000 K as compared to that of $SrTiO_3$, which is likely due to an enhanced phonon scattering at the $SrO/(SrTiO_3)_n$ ($n=1,2$) interfaces. The DOS effective mass m_d^* (1.8–2.4 m_0) and consequently the Seebeck coefficient $|S|$ in Nb^{5+}-doped samples are fairly smaller than those reported for $SrTiO_3$, which probably results from a deterioration of DOS due to the formation of the singly degenerate a_{1g} (Ti $3d_{xy}$) orbital as the conduction band bottom induced by the distortion of TiO_6 octahedra in $(SrTiO_3)_n$ layers. However, in the Ln^{3+}-doped $SrO(SrTiO_3)_2$, the TiO_6 octahedra were found to be restored, in contrast to the Nb^{5+}-doped, with a gradually increasing O–Ti–O bond angle in the (100) plane at high temperatures, which would lead to the formation of triply degenerate Ti $3d$-t_{2g} (d_{xy}, d_{yz}, and d_{xz}) orbitals to cause a significant enhancement in m_d^* (~7.5 m_0 at 1000 K) and consequently in $|S|$. Accordingly, the maximum dimensionless figure of merit $ZT \sim 0.24$ obtained in 5%-Gd^{3+}-doped $SrO(SrTiO_3)_2$ at 1000 K is about 70% larger than that of Nb-doped $SrO(SrTiO_3)_2$ ($ZT_{1000\ K} \sim 0.14$).

For further improvement of the TE properties of RP phases, the bottleneck is considered to be the effect of electrical barrier of SrO layers that are randomly distributed in the polycrystalline ceramics since the Seebeck coefficient can be enhanced by the restoration of TiO_6 octahedra through small-sized-Ln-doping. More efforts are to be made on the preparation of highly c-axis-oriented textured ceramics, single crystals, and RP compounds with a larger n in $SrO(SrTiO_3)_n$ to achieve a higher electrical conductivity. In addition, these compounds probably suffer from being oxidized during their use in the air, and some protective techniques, e.g., encapsulation, must be developed for practical application.

ACKNOWLEDGMENTS

We all the authors are deeply indebted to Dr. Hideki Hyuga and Dr. Hideki Kita at National Institute of Advanced Industrial Science and Technology (AIST), Japan, for their technical support in hot-pressing process and to Dr. Katsuhiko Inaba (Rigaku Co.) for his great job of high temperature XRD measurements. Meanwhile, the first author would like to express his heartfelt gratitude to Nature COE program and Global COE program of Nagoya University for their financial support during the research.

[1] T. Okuda, K. Nakanishi, S. Miyasaka, and Y. Tokura, Phys. Rev. B **63**, 113104 (2001).
[2] S. Ohta, T. Nomura, H. Ohta, M. Hirano, H. Hosono, and K. Koumoto, Appl. Phys. Lett. **87**, 092108 (2005).
[3] S. Ohta, T. Nomura, H. Ohta, and K. Koumoto, J. Appl. Phys. **97**, 034106 (2005).
[4] D. Kurita, S. Ohta, K. Sugiura, H. Ohta, and K. Koumoto, J. Appl. Phys. **100**, 096105 (2006).
[5] K. H. Lee, S. W. Kim, H. Ohta, and K. Koumoto, J. Appl. Phys. **100**, 063717 (2006).
[6] I. Terasaki, Y. Sasago, and K. Uchinokura, Phys. Rev. B **56**, R12685 (1997).
[7] M. Shikano and R. Funahashi, Appl. Phys. Lett. **82**, 1851 (2003).
[8] H. Ohta, W. S. Seo, and K. Koumoto, J. Am. Ceram. Soc. **79**, 2193 (1996).
[9] S. N. Ruddlesden and P. Popper, Acta Crystallogr. **10**, 538 (1957).
[10] S. N. Ruddlesden and P. Popper, Acta Crystallogr. **11**, 54 (1958).
[11] L. F. Mattheiss, Phys. Rev. B **6**, 4718 (1972).
[12] T. Schimizu and T. Yamaguchi, Appl. Phys. Lett. **85**, 1167 (2004).
[13] Y. F. Wang, K. H. Lee, H. Hyuga, H. Kita, K. Inaba, H. Ohta, and K. Koumoto, Appl. Phys. Lett. **91**, 242102 (2007).
[14] Y. F. Wang, K. H. Lee, H. Ohta, and K. Koumoto, Ceram. Int. **34**, 849 (2008).
[15] C. Noguera, Philos. Mag. Lett. **80**, 173 (2000).
[16] G. Amow and S. J. Skinner, J. Solid State Electrochem. **10**, 538 (2006).
[17] M. Burriel, G. Garcia, M. D. Rossell, A. Figueras, G. Van Tendeloo, and J. Santiso, Chem. Mater. **19**, 4056 (2007).
[18] F. Izumi and T. Ikeda, Mater. Sci. Forum **321–324**, 198 (2000).
[19] R. D. Shannon, Acta Crystallogr., Sect. A: Cryst. Phys., Diffr., Theor. Gen. Crystallogr. **32**, 751 (1976).
[20] K. H. Lee, S. W. Kim, H. Ohta, and K. Koumoto, J. Appl. Phys. **101**, 083707 (2007).
[21] M. Sánchez-Andújar and M. A. Señarís-Rodríguez, Z. Anorg. Allg. Chem. **633**, 1890 (2007).
[22] L. J. Knott, N. J. Cockroft, and J. C. Wright, Phys. Rev. B **51**, 5649 (1995).
[23] P. D. Battle, M. A. Green, N. S. Laskey, J. E. Millburn, L. Murphy, M. J. Rosseinsky, S. P. Sullivan, and J. F. Vente, Chem. Mater. **9**, 552 (1997).
[24] R. Asahi, Y. Taga, W. Mannstadt, and A. J. Freeman, Phys. Rev. B **61**, 7459 (2000).